Aerothermodynamic Environment about a Highly Swept Wing Leading Edge

Iraj Amirkabirian* and John J. Bertin†
University of Texas at Austin, Texas
and
Sam A. Mezines‡
McDonnell-Douglas Astronautics Company, St. Louis, Missouri

A numerical code has been developed to predict the aerothermodynamic environment of a highly swept wing leading edge at zero angle of attack, including the region outboard of the shock/shock intersection and a real-gas model for the thermodynamic properties as well as a perfect-gas model. Flowfield solutions generated by the code have been compared with wind tunnel data for wedge/swept-cylinder configurations and for the Space Shuttle Orbiter at zero angle of attack. The agreement between the computed flowfields and the experimental data is consistent with the approximations tacit to the flowfield model used in the numerical code. Furthermore, the computed heating rate histories for the wing leading edge at station $2y_B/b = 0.55$ are in reasonable agreement with the stagnation line flight measurements, even though the data for the flight are at an angle of attack while the computed values are for zero angle of attack.

Nomenclature

b = wing span
L = length of the vehicle
n = normal to the streamline
p = static pressure
r = radial distance from the centerline of the cylinder representing the wing leading edge
r_k = radius of curvature
w = transverse velocity
ϕ = circumferential angle in a plane normal to the wing leading edge

Subscripts

∞ = freestream
sl = stagnation line

Introduction

TO generate design values for the convective heating rates experienced by a maneuvering vehicle during re-entry, one must be able to develop engineering models for the viscid/inviscid interactions associated with complex three-dimensional flowfields. One such viscid/inviscid interaction that has received considerable attention because of its importance to the Space Shuttle Orbiter is that interaction between the fuselage-generated shock envelope and the wing-generated shock envelope that can produce large perturbations in the local heating to the wing leading edge.

It has been observed that hypersonic vehicles can experience severe damage from locally high heating rates generated when the incident, or "bow," shockwave of the vehicle impinges on the leading edge of a wing or a fin. The problems of shock-wave/boundary-layer interference have been widely studied in recent years. Many of the investigations employed a shock generator (either a wedge or conical surface) to generate the bow shock wave and a fin with a hemicylindrical leading edge to represent the wing. Thus the models were designed to simulate the essential features of the flight configurations while providing a flowfield which could be readily analyzed.

Bushnell[1] correctly identified the flowfield phenomena associated with the intersection of the "bow-generated" shock wave with the cylinder-generated shock wave for very large sweep angles. Edney[2] classifies this interaction as a Type VI pattern. No localized increases in heating were measured in the region of the wedge shock impingement for either laminar or turbulent stagnation-line, boundary-layer flow. However, the heating increased along that portion of the cylinder subjected to the wedge flow. The maximum increase in this region can be predicted using the local flow conditions to evaluate the necessary fluid properties for the infinite, swept-cylinder theories.[3] By comparing the data obtained when the cylinder and the wedge were attached with the data obtained when the cylinder and the wedge were separated, Bushnell found that the extent of the flow separation in the cylinder/wedge juncture was small for the flow conditions considered. Hiers and Loubsky[4] observed the same general features in data obtained at a very much lower Reynolds number.

From these tests involving "partial" models, one finds that the important parameters in describing the interaction between the bow shock wave and the wing shock wave include the initial flow deflection (i.e., the incidence angle of the shock generator), the sweep angle of the leading edge, the Mach number, and the Reynolds number.

Since the flowfields for winged configurations contain multiple shock envelopes, interactions between two or more of the shock waves generate the viscid/inviscid interactions already described. The intensity of the interaction phenomena between the fuselage-generated shock wave and the wing-generated shock wave is strongly configuration-dependent. Flowfield perturbations are much more pronounced for the straight-winged, low cross-range orbiters than for the delta-winged, high cross-range orbiters.

Solutions have been developed for the "three-dimensional" flow in the plane of symmetry of a swept cylinder (which represented the wing leading edge) that was mounted on a wedge (which generated the bow shock wave). A numerical

Presented as Paper 86-0389 at the AIAA 24th Aerospace Sciences Meeting, Reno, NV, Jan. 6-9, 1986; received Feb. 19, 1986; revision received June 7, 1986.

*Research Associate, Department of Aerospace Engineering and Engineering Mechanics. Member AIAA.
†Bettie Margaret Smith Professor of Engineering, Department of Aerospace Engineering and Engineering Mechanics. Fellow AIAA.
‡Section Chief Technology, McDonnell-Douglas Astronautics Co. Member AIAA.

code was developed[5] using integral techniques to calculate the flow in the shock layer upstream of the interaction region (i.e., near the wing root). Heat transfer rates were calculated for various freestream conditions, including the re-entry flight conditions expected for the Shuttle Orbiter. A velocity-dependent increase was observed in the computed heating rates in the region inboard of the interaction. The analyses of Refs. 5 and 6 were used by designers at Rockwell to develop a scaling correlation from wind tunnel-measured data to the anticipated flight conditions.[7]

The work described in the present paper was undertaken to extend these techniques to calculate the aerothermodynamic environment for the wing leading edge in the interaction region and beyond.

Analysis

As was noted in the Introduction, the type of shock interaction pattern that occurs when the bow-generated shock intersects the wing leading edge shock wave is governed primarily by the sweep angle of the leading edge. Since the Type VI pattern most probably exists for the highly swept leading edges of current interest, the subsequent analysis will be limited to this type of interaction. A detailed sketch of the flowfield model for this pattern is presented in Fig. 1.

Flowfield Adjacent to the Wedge (Region 2)

The simulated bow shockwave is generated when a wedge deflects the freestream flow through an angle δ. For this assumed flow model, the bow shock wave is linear and the flow in Region 2 is two-dimensional. Thus, for the present flow model, a particular property is constant throughout this region. With the freestream conditions and the flow deflection angle δ known, the Rankine-Hugoniot relations[8] can be used to uniquely determine the flow properties in Region 2. The real-gas properties for air in thermodynamic equilibrium are generated using a table lookup procedure based on the Mollier tables[9] or using a series of curve fits.[10]

Flow along the Wing Leading Edge

Since only the Type VI shock/shock interaction is to be considered, the cylinder, i.e., the simulated wing leading edge, is inclined relative to the wedge such that the flow downstream of the wing leading edge shock envelope remains supersonic. Crossflow away from the plane of symmetry causes the flow in the shock layer to be three-dimensional. As a result, the wing leading edge shock envelope is curved. The streamtube method is used in the present study to calculate the effects of crossflow on the shock structure and the fluid properties in the shock layer along the wing leading edge.

Sketches of the streamtube patterns that were used to calculate the inviscid flowfield in the plane of symmetry inboard of the shock/shock interaction are presented in Figs. 2 and 3. Note that the wing leading edge shock wave begins at the juncture between the wedge (i.e., the simulated fuselage) and the cylinder (i.e., the simulated wing). Thus, the effect of the fuselage boundary layer and the possibility that the viscid/inviscid interaction causes separation at the wing root are not included in the flow model. This omission could be of importance at very low Reynolds numbers (where the fuselage boundary layer would be sensitive to shock-induced perturbations) or for extreme sweep angles (either very low or very high, yet within the range of Type VI).

The inviscid shock-layer flow is computed for a grid of fluid elements (i,j) where i designates the streamwise station and j designates the streamtube. Downstream of the shock wave, the entropy is assumed to be constant along a streamline.

The procedure begins with the element at the wing root of the swept cylinder, i.e., element (1,1), and proceeds downstream. Sketches illustrating the nomenclature for this segment are presented in Figs. 4 and 5. The crossflow velocity for the fluid leaving the element (see Figs. 3, 5, and 6) is

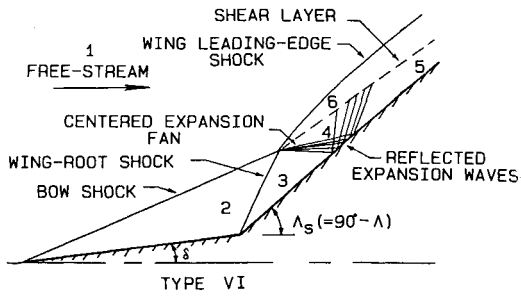

Fig. 1 Flow model of the shock interaction pattern for wedge cylinder.

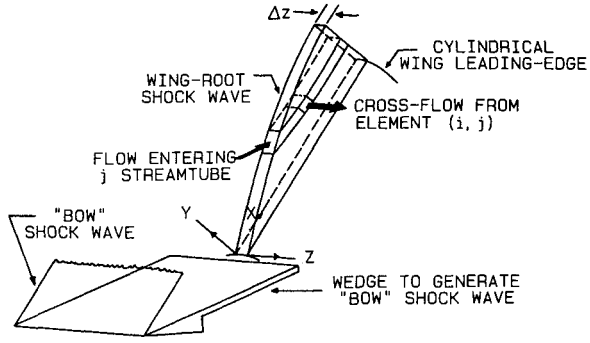

Fig. 2 Sketch of the theoretical model for the flowfield inboard of the shock/shock interaction, i.e., Region 3.

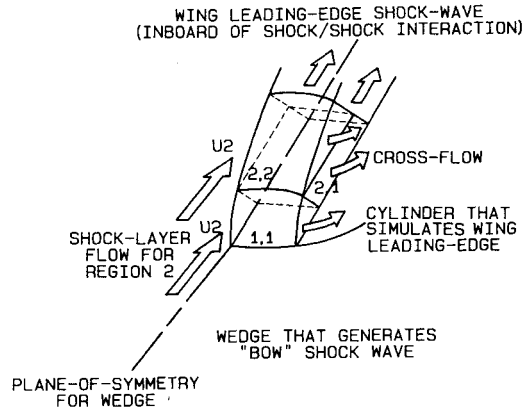

Fig. 3 A detailed sketch of the mass balance concept for the streamtubes in the wing root region.

calculated using the linear approximation

$$w = \frac{dw}{dz}\Delta z \tag{1}$$

The required crossflow velocity gradient is determined assuming that the pressure variation perpendicular to the stagnation line (i.e., the plane of symmetry) is approximately that for a modified Newtonian flow. Furthermore, the modified Newtonian pressure correlation is simplified to the form

$$\frac{p}{p_{sl}} = \cos^2\phi \tag{2}$$

because ϕ is small and p_∞/p_{sl} should be much less than one.

Using Euler's equation to approximate the inviscid flow in the transverse plane

$$\left(w\frac{dw}{dz}\right)_{sl} = -\left(\frac{1}{\rho}\frac{dp}{dz}\right)_{sl} \tag{3}$$

and taking the derivative of Eq. (2),

$$\frac{dp}{dz} = -2p_{sl}\cos\phi\sin\phi\frac{d\phi}{dz} \tag{4}$$

Combining Eqs. (1), (3), and (4) and noting that ϕ is small near the stagnation line, the required velocity gradient is

$$\left(\frac{dw}{dz}\right)_{sl} = \left(\frac{1}{r}\sqrt{\frac{2p}{\rho}}\right)_{sl} \tag{5}$$

These equations are applied not only to element (1,1) but to all elements.

Using the nomenclature of Figs. 4 and 5, a mass balance is written for the wedge-like element (1,1). An iterative procedure for the shock wave angle is repeated until the mass efflux is within 1% of the mass influx for this element. Having satisfied this criterion, the shock wave angle and the flow properties for the first element (1,1) are calculated preparatory to solving for the flow in the elements of the second station $(2, j)$ where $j = 1$ or 2.

As shown in Fig. 3, there are two elements at the second streamwise station: a wedge-like element bounded by the wing leading edge shock wave (2,2) and a rectangular element adjacent to the wall (2,1). The final value of the shock wave angle for element (1,1) is used as the initial guess for the shock wave angle for the second streamwise station. Since the flow properties upstream of the shock wave (i.e., in Region 2) are known, the static pressure and the flow direction for element (2,2) can be calculated. For the initial iteration, the pressure is assumed to be constant across the shock layer, i.e., independent of y. The entropy of the fluid of the internal element (2,1) is assumed to be equal to that of element (1,1); i.e., the entropy is constant along a streamline. Having determined the pressure and the entropy, the remaining fluid properties can be evaluated.

The flow direction in element (2,1) is specified as being parallel to the wall, whereas the flow direction in element (1,1) is defined by the resultant shock wave angle. The change in the flow direction is used to construct the streamline and to calculate its radius of curvature. Since the pressure gradient normal to the streamline[11] is

$$\frac{\partial p}{\partial n} = \frac{\rho U^2}{r_k} \tag{6}$$

Thus, one can estimate the pressure gradient across an element in the shock layer. With the static pressure in the element immediately downstream of the shock wave (2,2) defined by the Rankine-Hugoniot relations, the pressure change across the shock layer is calculated using Eq. (6) to account for the curvature of the inner streamline. Since the assumption that the entropy is constant along a streamline remains in force, the other flow properties of element (2,1) can be calculated.

Using the "improved" flow properties, the mass balance requirement is applied to the rectangular element as shown in Fig. 6. If the mass efflux calculated is not within 1% of the mass influx, the shock wave angle is corrected, and the iterative procedure for calculating the pressure distribution across the shock layer is repeated. The calculation of the mass flux for the rectangular element and of the pressure distribution across the shock layer is repeated until successive values of the surface pressure agree to within 0.1%.

A similar procedure was used at successive streamwise stations up to the location where the simulated bow shock wave intersected the wing leading edge shock wave.

Outboard of the Shock/Shock Intersection

Note that the flow that passes through the wing leading edge shock wave outboard of the intersection with the bow shock wave passes through a single shock wave (see Fig. 1). At the same station, the fluid that is near the surface has passed through two shock waves. Note that all of the shock waves in the Type VI pattern are weak; that is, the downstream flow remains supersonic (with limited exceptions). Thus, since the turning of a flow through incremental steps causes the static pressure to be greater than it would be if the same turning were accomplished in a single step, the static pressure in Region 3 (inboard of the intersection) is greater than that in Region 6 (outboard of the intersection). To accomplish the required pressure decrease, an expansion fan originates at the shock/shock intersection and impinges on the wing leading edge as shown in Figs. 1 and 7. The acceleration of the fluid along a streamline is isentropic as the fluid particles go from Region 3 through Region 5. As a result, the entropy of the fluid in Regions 3 through 5, i.e., that fluid passing through two shock waves, is less than the entropy of the fluid in Region 6, which has passed through a single (albeit, relatively strong) shock wave.

At a given station, the pressure and the flow direction at the outer portion of Region 4 (initially, and Region 5, eventually) match those of the inner bound of Region 6. However, the variation in entropy causes differences in other fluid properties (e.g., velocity) as well. Thus, a shear layer at the interface between the flow in these two regions originates at the shock/shock intersection. If one neglects the viscous effects that create the shear layer (as was done in the present study), a slip line (or a discontinuity in fluid properties) originates at the intersection.

A single wave is used for the expansion process in the present model for flow past the swept cylinder that represents the wing leading edge. This flow model simplification allows the

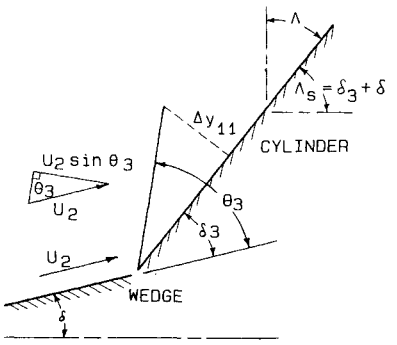

Fig. 4 Nomenclature for the wing leading edge/shock wave structure in the wing root region.

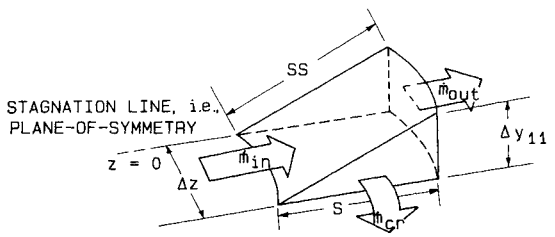

Fig. 5 Sketch illustrating the mass balance for the wedge-like element (1,1) at the wing leading region.

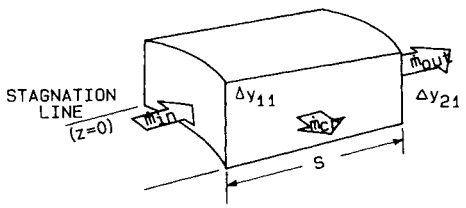

Fig. 6 Sketch illustrating the mass balance for rectangular element (2,1).

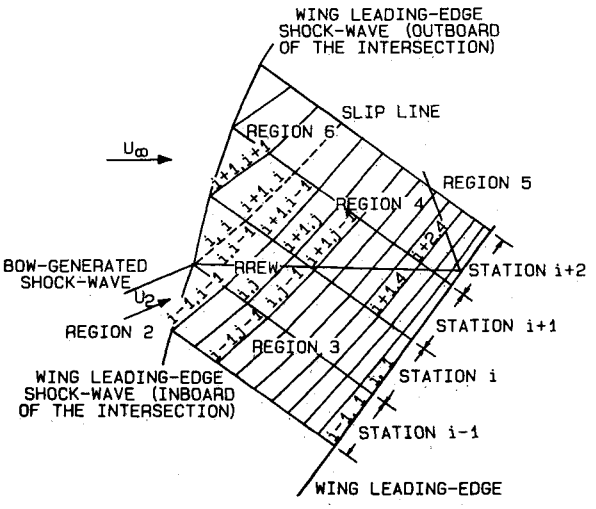

Fig. 7 Nomenclature for the flow containing the expansion wave and its reflection.

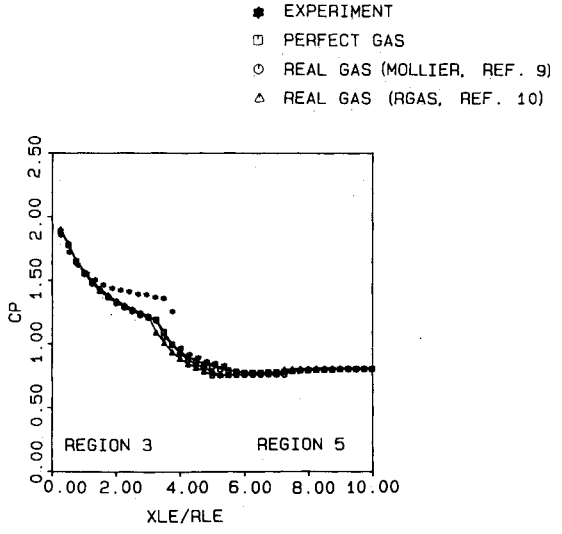

Fig. 8 A comparison of the computed pressure distributions and the experimental pressures for $\Lambda = 45$ deg, as presented in Ref. 15.

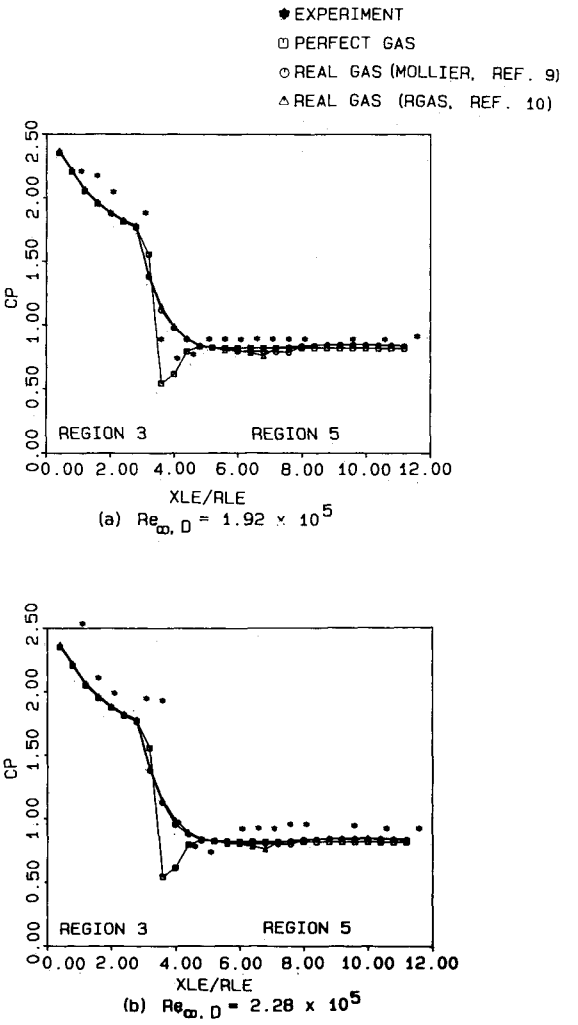

Fig. 9 Plane of symmetry pressure distribution for wedge/cylinder configuration of Ref. 1, $\Lambda = 45$ deg.

mass balance (including crossflow) for the elements to be more easily calculated while maintaining an accuracy consistent with this technique. Again, the iterative procedure employs the calculation of the streamline curvature, the computation of the pressure gradient across the shock layer, and the application of the mass-flow-balance requirement to solve for the inviscid shock-layer flow. The iterative procedure is repeated until successive values of the surface pressure agree to within 0.1%.

The reflected expansion wave is assumed to be of equal strength to the impinging wave but is a left-running wave. Once the reflected expansion wave encounters the wing leading edge shock wave, it is cancelled, and no further waves cross the shock layer. Thus, the computation of the flow downstream of this station is identical to the procedure described for the flow inboard of the shock/shock intersection.

Heat Transfer Distribution along the Wing Leading Edge

The heat transfer distribution for the plane of symmetry of the swept cylinder was calculated using a code for a nonsimilar boundary layer.[12] In order to generate solutions for the viscous boundary layer, one must input the flow properties at the edge of the boundary layer and the flow properties at the wall. The three-dimensional character of the boundary layer is approximated using the axisymmetric analog.[13] Thus, another input is the cross-section radius for the equivalent body of revolution. The inviscid, shock-layer flowfield (determined using the techniques of the previous sections) provides the flow properties at the edge of the boundary layer. The wall temperature distribution is assumed to be known, providing the boundary condition at the inner edge of the boundary layer.

The divergence of the streamlines along the wing leading edge is characterized by the metric coefficient distribution, i.e., the streamwise variation of the cross-sectional radius for an equivalent body of revolution. The metric coefficient distribution is calculated using the relation[14]

$$dr_{eq} = \frac{r_{eq}}{u}\frac{dw}{dz}dx \tag{7}$$

The radius of the cylindrical leading edge is used as the value of the metric of the initial streamwise station, i.e., at the wing root station.

Heat transfer distributions along the plane of symmetry were calculated for a laminar boundary layer originating either at the upstream end of the cylinder or at the leading edge of the wedge. For this latter procedure, which was used in generating solutions for "Space Shuttle-like" configurations, the flow over the wedge is assumed to be two-dimensional and that along the cylinder leading edge to be equivalent axisymmetric.

Discussion of Results

The numerical code has been used to compute the flowfield solutions for various wedge/swept-cylinder configurations exposed to a variety of flow conditions. For those configurations for which data are available, the computed flowfields are compared with the experimental values.

Correlations with Data from Ref. 15

Schlieren photographs and surface pressure measurements were obtained when a wedge/cylinder configuration was exposed to a supersonic stream by Barnette.[15] The freestream Mach number was 4.97 and the nominal freestream Reynolds number was 51.7×10^6/m (15.7×10^6/ft). The sweep angle of the cylinder was varied from 30 through 70 deg.

The measured pressures are compared with the computed values in Fig. 8. Computed flowfield solutions were generated for three models for these gas properties: perfect-gas, air in thermodynamic equilibrium as defined by the Mollier tables,[9] and air in thermodynamic equilibrium as defined by correlations.[10] Since air at wind tunnel conditions behaves as a perfect gas, the computed solutions are essentially the same for all three gas models.

Correlations with Data from Ref. 1

Surface pressures generated using the computer code have been compared with the corresponding experimental values that are presented by Bushnell.[1] The models used in the experimental program consisted of a sharp flat-plate inclined at a 12 deg angle to the freestream flow and circular cylinders that were either attached to or separated from the wedge and were swept either 45 or 60 deg to the freestream.

The computed and the measured pressure distributions from the plane of symmetry are compared in Fig. 9 for $\Lambda=45$ deg. As is the case with the data of Barnette,[15] the computed flowfield provides satisfactory values for the pressures near the wing root, for the location of the impinging expansion fan, and for the pressures in the region downstream of the interaction. The correlation between the computed pressures and the measured values is weakest at the downstream end of Region 3.

Space Shuttle Orbiter

The computer code was used to generate flowfield solutions for a wedge/cylinder geometry in an attempt to develop correlations for the wing leading edge of the Space Shuttle Orbiter. Flowfield solutions were generated for the freestream conditions of the wind tunnel tests described in Ref. 16 using the perfect-gas relations for the properties of air and for the flight environments[19] using different models for the properties of air.

Correlations of the Wind Tunnel Results

Heat transfer rates were measured on an 0.025-scale model of the Space Shuttle Orbiter in the Calspan Hypersonic Shock Tunnel.[16]

The computer code was used to generate flowfield solutions for a wedge/cylinder configuration. The planforms of the Shuttle Orbiter configuration and of the wedge/cylinder configuration used to model the flow in the computer code are presented in Figs. 10a and 10b respectively. As shown in Fig. 10b, the wedge was inclined 9 deg to the freestream flow, thus matching the planform inclination angle of the fuselage. The cylinder was swept 45 deg, matching the wing leading edge sweep angle. Note that the wedge/cylinder geometry does not simulate the gradual turning of the flow in the wing root region produced by the glove on the Orbiter (the planform trace of which is indicated by the broken line of Fig. 10b).

The computed heat transfer distribution for the wedge/cylinder configuration described is compared in Fig. 11 with the heating rates measured in the Calspan Hypersonic Shock Tunnel using an 0.025-scale Orbiter at zero angle of attack.[16] The heat transfer rates for the fuselage and for the wing leading edge are presented as a function of x_B/L. Thus, a

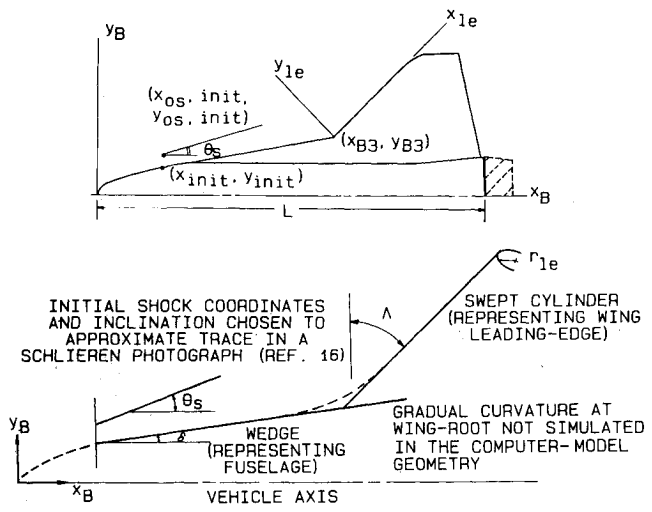

Fig. 10 Sketch of the nomenclature for the coordinate systems used in the computer model: a) coordinate system for the Space Shuttle Orbiter; b) coordinate system for the wedge/cylinder configuration.

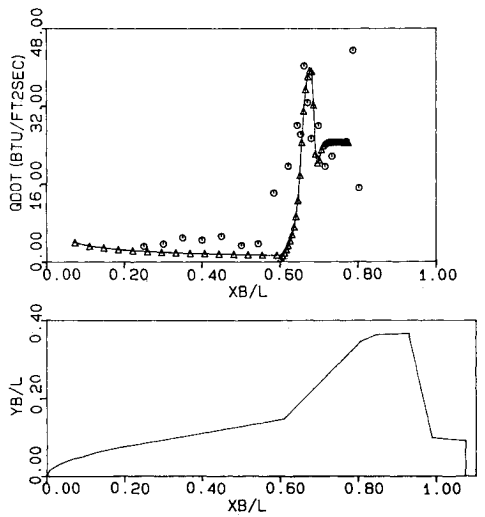

Fig. 11 Comparison of computed heat transfer distribution with experimental measurements of Ref. 16 for $\alpha=0$ deg, $M_\infty=9.857$, $Re_{\infty/ft}=1.584\times10^6$.

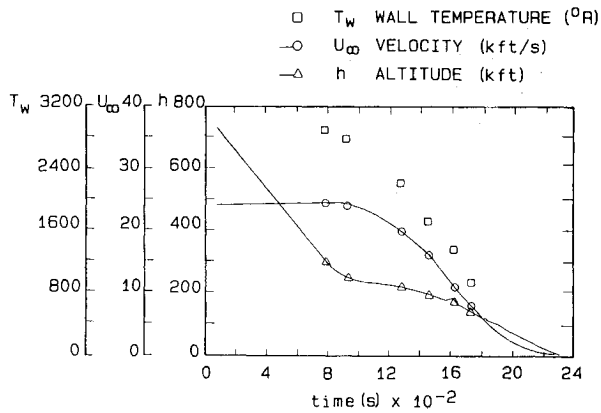

Fig. 12 Histories of flight parameters for STS4 as a function of time from epoch (Ref. 18).

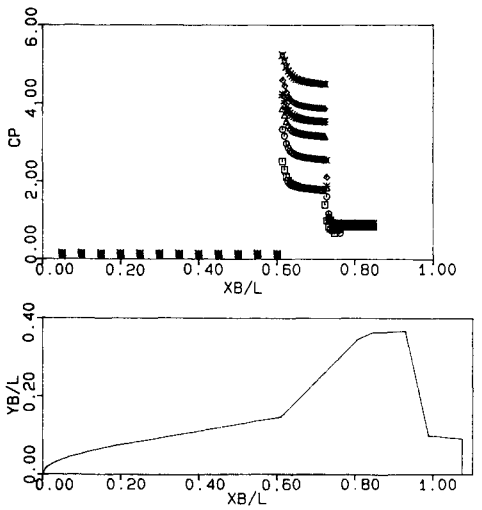

a)

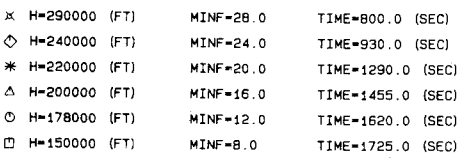

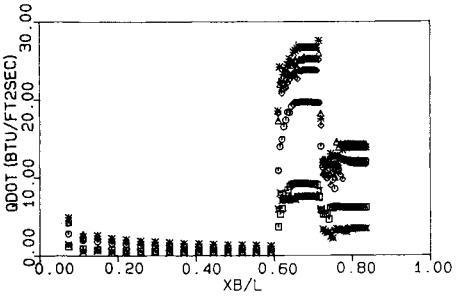

b)

Fig. 13 Pressure and heat transfer distributions for six selected flight conditions: a) pressure distributions; b) heat transfer distributions.

sketch of the model planform is included in Fig. 11 to provide a physical reference for the heating rate distribution. The freestream Reynolds number based on a wing leading edge diameter of 1.27 cm (0.50 in.), which is the approximate leading edge diameter at $2y_B = 0.55b$ and which serves as the "reference value" for the present discussion of the wind tunnel data, is 0.66×10^5. Based on Bushnell and Huffman's transition criteria for swept cylinders or for wing leading edges,[17] the boundary layer should be laminar for this case. The "reasonable" agreement between the theoretical laminar values and the experimental values substantiate this assumption.

Correlations at Flight Conditions

Flowfield solutions for the wing leading edge were also generated for flight conditions. The dimensions of the wedge/cylinder configuration used in the computer model simulated the full-scale Shuttle Orbiter. Six conditions were selected from the velocity/altitude histories for the flight of the STS4, as presented in Ref. 18. The trajectories from Ref. 18 and the six flight conditions selected for further analysis are presented in Fig. 12. Also presented in Fig. 12 are the assumed wall temperatures at the times of interest. The wall temperature histories are based on flight-test data presented by Curry et al.[19]

The pressure distributions and the heat transfer distributions from the plane of symmetry are presented in Figs. 13a and 13b. To account for the real-gas effects, the thermodynamic properties were determined using the relations[10]

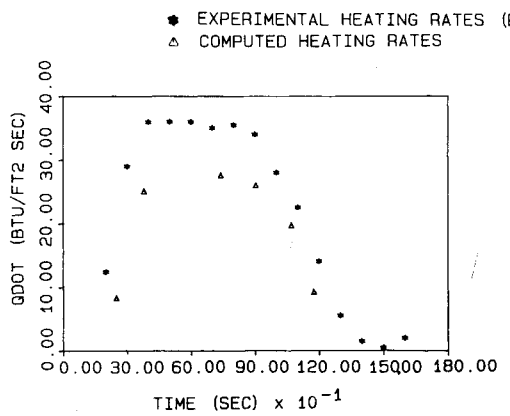

Fig. 14 Comparison of computed heating rates and the measured nominal flight heating rate history for panel 9 (Ref. 19).

for the inviscid flow and the tables[9] for the boundary-layer calculations.

The heat transfer distributions for the six selected conditions are presented in Fig. 13b. The heat transfer rates apparently exhibit an interrelated dependence on the various parameters, e.g., freestream conditions, surface temperature, etc. As a result, without experimental data to compare with these computed heat transfer distributions, no further comments will be made regarding Fig. 13b. However, Curry et al.[19] present heating rate histories at selected locations from the flight of STS2. The nominal heating rate history for panel 9 presented by Curry et al. is reproduced in Fig. 14. Also presented are the heating rates at this location computed for six selected flight conditions. Note that in order to align the two heating rate histories (i.e., to match the time of the relatively constant heating rates), 550 s were subtracted from the time scale of Fig. 12. The agreement between the computed values and the experimental values presented in Fig. 14 is considered good. However, in a subsequent analysis of these data, Williams and Curry[20] note that "the Panel 9 convective heating has been arbitrarily increased to obtain better agreement between measured and predicted temperatures." Thus, the reader should view the correlation between the present calculations and the flight data as presented in Fig. 14 as qualitative.

Concluding Remarks

A numerical code has been developed to compute the aerothermodynamic environment for a Type VI shock/shock interaction for a wedge/swept-cylinder configuration. The flow model also approximates that for the wing leading edge of a configuration at zero angle of attack. The code has been used to generate flowfield solutions for wedge/cylinder configurations in a variety of wind tunnel environments. Comparisons were made between data and theory for schlieren photographs, surface pressures, and heat transfer rates. The code has also been used to generate flowfield solutions for the Space Shuttle Orbiter at wind tunnel conditions and at flight conditions. The agreement between the computed flowfields and the experimentally determined values for the various parameters is believed to be acceptable over the entire range of conditions considered.

Acknowledgments

The authors would like to express their appreciation to the McDonnell-Douglas Corporation for supporting this work through Purchase Order Y3E135. The authors would like to acknowledge the contributions of Richard Neumann of the Department of the Air Force.

References

[1]Bushnell, D. M., "Interference Heating on a Swept Cylinder in Region of Intersection with a Wedge at Mach Number of 8," NASA TN D-3094, Dec. 1965.

[2]Edney, B., "Anomalous Heat Transfer and Pressure Distributions on Blunt Bodies at Hypersonic Speeds in the Presence of an Impinging Shock," Flygteckniska Forsoksanstalten (The Aeronautical Research Institute of Sweden), Rept. 115, 1968.

[3]Beckwith, I. E. and Gallagher, J. J., "Local Heat Transfer and Recovery Temperature on a Yawed Cylinder at a Mach Number of 4.15 and High Reynolds Number," NASA TR R-104, 1961.

[4]Hiers, R. S. and Loubsky, W. J., "Effects n Shock-Wave Impingement on the Heat Transfer on a Cylindrical Leading Edge," NASA TN D-3859, Feb. 1967.

[5]Bertin, J. J., Mosso, S. J., Barnette, D. W., and Goodrich, W. D., "Engineering Flow Fields and Heating Rates for Highly Swept Leading Edges," *Journal of Spacecraft and Rockets*, Vol. 13, Sept. 1976, pp. 540-546.

[6]Bertin, J. J., Graumann, B. W., and Goodrich, W. D., "High Velocity and Real-Gas Effects on Weak Two-Dimensional Shock-Interaction Patterns," *Journal of Spacecraft and Rockets*, Vol. 12, March 1975, pp. 155-161.

[7]Cunningham, J. A. and Haney, J. W. Jr., "Space Shuttle Wing Leading Edge Heating Environment Prediction Derived from Development Flight Data," NASA CP-2283 Part II, "Shuttle Performance: Lessons Learned," March 1983.

[8]Bertin, J. J., *Engineering Fluid Mechanics*, Prentice-Hall, Inc., New York, 1979.

[9]Moeckel, W. E. and Weston, K. C., "Composition and Thermodynamic Properties of Air in Chemical Equilibrium," NACA TN 4265, April 1958.

[10]Eaton, R. R. and Larson, D. E., "Improved Real Gas Routines for Sandia's NASA Ames Flow Field Program," Sandia Laboratories, Albuquerque, NM, SAND75-0493, 1975.

[11]Shapiro, A. H., *The Dynamics and Thermodynamics of Compressible Fluid Flow*, Vol. 1, The Ronald Press Company, New York, 1953.

[12]Stalmach, D. D. and Bertin, J. J., "The Analysis of a Nonsimilar Laminar Boundary Layer," University of Texas at Austin, Aerospace Engineering Rept. 78001, Feb. 1978.

[13]Cooke, J. C., "An Axially Symmetric Analogue for General Three-Dimensional Boundary Layers," British Aeronautical Research Council R & M 3200, 1961.

[14]Rakich, J. V. and Mateer, G. G., "Calculation of Metric Coefficients for Streamline Coordinates," *AIAA Journal*, Vol. 10, Nov. 1972, pp. 1538-1540.

[15]Barnette, D. W., "An Experimental Investigation of Supersonic Flow Past a Wedge-Cylinder Configuration," University of Texas at Austin, Aerospace Engineering Rept. 76002, April 1976.

[16]Wittliff, C. E. and Berthold, C. L., "Results of Heat Transfer Testing of an 0.025-Scale Model (66-0) of the Space Shuttle Orbiter Configuration 140B in the Calspan Hypersonic Shock Tunnel (OH66)," Data Management Services, DMS-DR-22359 (NASA CR-151, 405), Jan. 1978.

[17]Bushnell, D. M. and Huffman, J. K., "Investigation of Heat Transfer to Leading Edge of a 76° Swept Fin With and Without Chordwise Slots and Correlations of Swept Leading-Edge Transition Data for Mach 2 to 8," NASA TMX-1475, 1967.

[18]Compton, H. R., Schiess, J. R., Suit, W. T., Scallion, W. I., and Hudgins, J. W., "Stability and Control over the Supersonic and Hypersonic Speed Range," *Shuttle Performance: Lessons Learned*, Part I, NASA CP 2283, March 1983.

[19]Curry, D. M., Latchem, J. W., and Whisenhunt, G. B., "Space Shuttle Orbiter Leading Edge Structural Subsystem Development," AIAA 83-0483, presented at the AIAA 21st Aerospace Sciences Meeting, Reno, NV, Jan. 1983.

[20]Williams, S. D. and Curry, D. M., "Assessing the Orbiter Thermal Environment Using Flight Data," *Journal of Spacecraft and Rockets*, Vol. 21, Nov.-Dec. 1984, pp. 534-541.